AuAg bimetallic nanoparticles: formation, silica-coating and selective etching

Benito Rodríguez-González,[a] Ana Sánchez-Iglesias,[a] Michael Giersig[b] and Luis M. Liz-Marzán*[a]

[a] *Departamento de Química Física, Universidade de Vigo, 36200 Vigo, Spain. E-mail: lmarzan@uvigo.es; Tel: +34 986812556*

[b] *Center of Advanced European Studies And Research (CAESAR), Ludwig-Erhard-Allee 2, 53175 Bonn, Germany*

Received 20th March 2003, Accepted 20th May 2003
First published as an Advance Article on the web 24th July 2003

A time-resolved study of the formation of AuAg alloy nanoparticles during boiling of $AgNO_3$ and $HAuCl_4$ in the presence of sodium citrate has been performed by monitoring the UV-visible spectra of the solutions. This study reveals clear differences with respect to the formation of pure Au particles, and suggests that gold and silver nanoparticles nucleate separately, but lattice rearrangement eventually leads to formation of alloy nanoparticles with the expected composition, which was confirmed by high resolution TEM. Additionally, we studied the chemical reaction of the alloy nanoparticles with NH_4OH, observing that part of the Ag atoms get oxidized, but reorganization of the crystal lattice during the reaction prevents full transformation into pure gold nanoparticles. This allows the synthesis of silica-coated bimetallic particles with tailored plasmon resonance between *ca.* 430 and 520 nm, as well as homogeneous incorporation of the coated alloy nanoparticles within silica gels.

1. Introduction

Metal nanoparticles are extremely interesting from both fundamental and practical points of view because of their size-dependent optical properties. For this reason, since Faraday's pioneering experiments,[1] many studies have been (and still are) devoted to the synthesis, modification, characterization and assembly of metallic[2–11] and bimetallic[12–18] nanoparticles in a wide variety of media. The origin of the optical properties of metal particles relies basically on the collective oscillation of conduction electrons (surface plasmon resonance) upon interaction with an incoming electromagnetic field.[19] The absorption and scattering from metal nanoparticle colloids can be predicted through the so-called Mie theory,[20] using as input parameters the wavelength-dependent, complex dielectric functions of the materials, calculated from the respective bulk data on the basis of the simple Drude model.[21–23] For some metals, such as Cu, Ag, Au, and the alkali metals, the frequency of the plasmon resonance lies within the visible range,[24] and this is the reason why colloidal dispersions of those metals display intense and beautiful colours. When two different metals are contained within a single nanoparticle, the resulting optical properties arise from a combined contribution of both metals, and the distribution of the metal atoms within the particle is of fundamental importance. Bimetallic nanoparticles with core-shell geometry have been studied

and their optical properties compared to calculations based on Mie theory.[13,16,25–29] Other authors explored the catalytic efficiency of bimetallic nanoparticles, as compared to nanoparticles of the pure metals.[17,30] The main second category of bimetallic nanoparticles is formed by the alloys. With respect to the optical properties, it was notable the work by Link *et al.*,[31] who showed that the spectra of AuAg alloy nanoparticles (formed by citrate reduction) could not be calculated correctly using an average of the dielectric constants of the pure metals. If the dielectric data for the bulk alloys was used instead, a good agreement between calculated and experimental spectra was obtained. Recently, Murphy *et al.*[32] demonstrated the formation of smaller alloy nanoparticles in a wide range of compositions *via* room-temperature reduction with borohydride.

The choice of Au and Ag for many studies on metal nanoparticles is due, apart from their intense plasmon resonance absorption and full miscibility, to their high chemical stability, so that they can be used in almost any environment with no risk of rapid chemical reactions. However, there are some reactions that such particles can undergo, and several examples have been described in the literature.[33] One specially disturbing limitation is the oxidation reaction of Ag nanoparticles catalysed by aqueous ammonia:

$$4Ag + 8NH_3 + O_2 + 2H_2O \rightarrow 4Ag(NH_3)_2^+ + 4OH^- \quad (1)$$

This reaction is the reason why Stöber synthesis[34] (silica formation by ammonia catalysed hydrolysis and condensation of alkoxysilanes) cannot be directly applied to the deposition of thick silica shells on small silver nanoparticles.[35] Gold nanoparticles are impervious to the same reaction, and thus thick silica shells have been deposited on Au nanoparticles without core etching,[36] and the coated nanoparticles used as building blocks for nanostructured materials.[37] This is a limitation for several applications, since the silver plasmon band is narrower, its extinction coefficient is *ca.* five times larger than that for gold, and the position of the band is typically 400 nm for Ag, while 520 nm for Au.[23]

The selective dissolution in (bulk) metal alloys (dealloying) is also of major importance in the context of corrosion studies. Sieradzki and co-workers[38] have studied this process for bulk samples and thin films, and modelled the dealloying process as a phase segregation, so that either small Au particles or porous gold can be formed depending on Au concentration within the alloy. These authors have also found that depending on the kinetics of the dissolution, the alloy can self-protect, in the sense that the Au atoms can rearrange on the surface, so that the interior cannot be reached by the outer solution.

In this paper we present a time-resolved study of the formation of AuAg alloy nanoparticles during their reduction by citrate ions, which aimed to disclose whether the alloy particles are formed from the start, or one of the metals forms first. We also studied the chemical reactivity of the alloys with respect to oxidation with ammonia for different molar ratios of the metals. Additionally, the alloy nanoparticles were coated with silica shells of various thicknesses, and homogeneously incorporated within silica gels.

2. Experimental

Chemicals

$HAuCl_4$, $AgNO_3$, trisodium citrate dihydrate, NH_4OH (30 wt.%) (3-aminopropyl)trimethoxysilane (APS), and sodium silicate solution ($Na_2O(SiO_2)_{3-5}$, 27 wt.% SiO_2) (all of them purchased from Aldrich) were used as received. Tetraethyl orthosilicate (TEOS) and tetramethyl orthosilicate (TMOS) (Aldrich) were distilled prior to use. Pure grade ethanol and methanol, and Milli-Q grade water were used in all the preparations. All other chemicals were analytical grade and used as supplied by the vendor.

Metal nanoparticles preparation

Pure Au and AuAg alloy nanoparticles were synthesised following the same procedure described by Link *et al.*[31] A constant total metal molar concentration of 0.5 mM was used, whilst the Au:Ag molar ratio was adjusted through the addition of the corresponding concentrations of $AgNO_3$ and $HAuCl_4$. To a boiling mixed solution of metal salts (100 mL), 5 mL of (preheated) sodium citrate 1

wt.% solution was added, and the boiling was continued for 30 min, being thereafter the solution allowed to cool down to room temperature.

Selective etching

The reaction of nanoparticles with ammonia was monitored within 10 mm path length quartz cuvettes, using a Hewlett-Packard HP8453 diode-array spectrophotometer equipped with a thermostated multiple sample holder. The cuvettes were filled with 2 mL of the colloid, to which 30 μL of concentrated ammonia were added and gently stirred for proper mixing.

Silica coating

A freshly prepared aqueous solution of APS (0.25 mL, 1 mM) was added to 100 mL of the bimetallic colloid under vigorous magnetic stirring. The mixture was then allowed to stand for 15 minutes and then 4 mL of a 0.54 wt% sodium silicate solution at pH ≈ 10.5–11 (adjusted with a cation exchange resin) was added, again under vigorous magnetic stirring. The resulting dispersion (pH ≈ 8.5) was then allowed to stand for four days, so that the active silica polymerised onto the primed metal particle surface. The silica shell thickness was about 3–5 nm thick after this period. The coated nanoparticles were subsequently transferred into ethanol (water:ethanol volume ratio = 1:4) under vigorous magnetic stirring and used as seeds for the growth of thicker shells, through addition of ammonia (0.35 M) and TEOS in small aliquots.

Sol–gel processing

In a typical preparation procedure, first 0.32 mL of TMOS was added to 1.33 mL of methanol. Next, 2 mL of a dispersion of alloy nanoparticles coated with a 3–5 nm thick silica shell, was added to the mixture of TMOS and methanol, and the final mixture was poured in a cuvette which was shielded with a rubber sheet to avoid unwanted evaporation. Upon several hours a rigid hydrogel was obtained. The final molar ratio of TMOS, water and methanol was 1:50:15, assuming that 2 mL of colloid contains 2 mL of water. Solid xerogel monoliths were obtained by drilling small holes in the shielding rubber sheet and allowing evaporation to take place on a time scale of 2–3 weeks.

Characterization techniques

Transmission electron microscopy (TEM) was carried out with a JEOL JEM-1010 microscope, while high-resolution transmission electron microscopy (HRTEM) was measured with a Philips CM12 microscope equipped with a high resolution lens and an elemental analysis system by X-ray energy dispersion (EDS) EDAX 9800. Sample preparation was performed by placing a drop of the dispersion on either carbon coated or FORMVAR-carbon coated copper grids and letting it dry in air. Time-resolved UV–visible spectroscopy was measured with a Hewlett-Packard HP8453 diode-array spectrophotometer, using a flow cell, which was fed from the boiling solution by means of a peristaltic pump. Full spectra (190–1100 nm) were recorded every 10 s with an integration time of 0.5 s.

3. Results and discussion

This section has been divided into four subsections. In the first one we discuss a study of the formation of AuAg alloy nanoparticles by *in situ* UV–visible spectroscopy and transmission electron microscopy. The selective etching of alloy nanoparticles of different compositions with ammonia is analyzed in the second subsection. Then we describe the deposition of uniform silica shells with tailored thickness, as well as the effect of silica coating on the optical properties of the composite nanoparticles, and the final section is devoted to the sol–gel processing of the alloy nanoparticles, which permits to obtain hydrogels and xerogels with tailored optical properties.

3.1. Formation of AuAg alloy nanoparticles

In previous studies[31,32] it was found that the position of the maximum of the surface plasmon band for AuAg alloy nanoparticles changes in a quasi-linear fashion between those for pure Ag and Au

colloids. Our study confirms this observation, although quantitative agreement was not achieved for all preparations. Examples of UV-visible spectra (normalized to unit absorbance at the maximum) for AuAg aqueous colloids with varying composition are shown in Fig. 1. The plasmon bands span the whole spectral range between 400 (pure silver) and 520 (pure gold) nm. Additionally, the intensity of the absorbance tail at low wavelengths (due to interband transitions and much more intense for gold) is also observed to be directly related to the gold content in the alloy nanoparticles. In the inset of Fig. 1 the measured maximum positions were plotted *versus* gold content within the particles, and compared to those reported by Link *et al.*[31] The positions of the plasmon bands were found to be reproducible within 3% only, which is probably related to different degrees of polydispersity for different preparations. The solid line in the inset is a linear fit to the theoretical values calculated using dielectric data for AuAg alloy films.[39] The calculation was performed by means of Mie theory,[20–23] neglecting scattering effects because of the small particle size, which leaves the following simple equation for the extinction coefficient:

$$C_{\text{ext}} = \frac{24\pi^2 R^3 \varepsilon_{\text{m}}^{3/2}}{\lambda} \frac{\varepsilon''}{(\varepsilon' + 2\varepsilon_{\text{m}})^2 + \varepsilon''^2} \tag{2}$$

where R is the particle radius, ε_{m} the dielectric constant of the solvent (water), λ the wavelength of the incident radiation, and ε', ε'' the real and imaginary parts of the dielectric function of the particle material, respectively. These values were taken from ref. 39.

The formation of alloy nanoparticles, rather than mixtures of Au and Ag nanoparticles is indicated by the presence of a single, well-defined plasmon band in the spectra. Additional confirmation was obtained by EDS, which was performed on several areas of the grid for each sample, and the beam was focused on a maximum of three nanoparticles for each analysis. These measurements confirm that the initial molar ratio defined through the amount of metal salts used is maintained within the particles, with an accuracy of ±1%. However, for Au contents below 20%, segregation was frequently observed, with formation of particles presumably made of an alloy core surrounded by a silver shell (see section 3.2).

We have chosen this synthetic method for our study in spite of yielding relatively polydisperse colloids because of the slower kinetics of formation (as compared to borohydride reduction), which allowed us to monitor the process of colloid formation. To this end, we performed a time-resolved study by means of UV–visible spectroscopy, using a diode-array spectrophotometer (see experimental section for details) with which complete spectra with 1 nm resolution can be measured

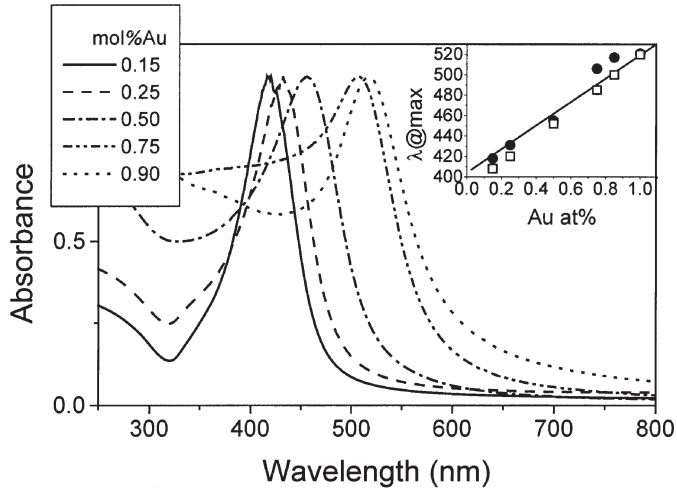

Fig. 1 Normalized UV–visible spectra of AuAg colloids with varying composition, as indicated. The inset shows the maximum position as a function of gold content. Solid circles correspond to this work, open squares to ref. 31 and the line is a linear fit to calculated values.

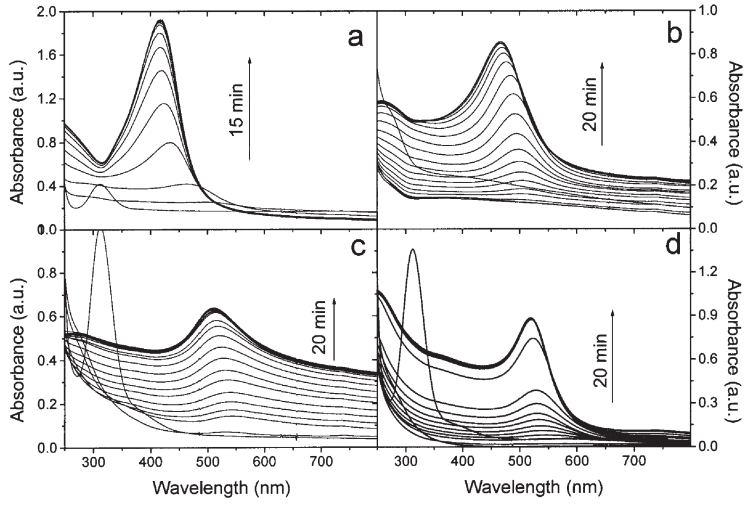

Fig. 2 Time evolution of UV-visible spectra during the formation of AuAg colloids by citrate reduction. The compositions are (Au at%) 25 (a), 50 (b), 75 (c), and 100 (d).

within tenths of a second. Since the synthesis was performed at high temperature (*ca.* 100 °C), spectra were measured by means of a flow cell to which the solution was introduced using a peristaltic pump and full spectra were measured every 10 s. Representative examples of the results obtained are shown in Fig. 2 for three different compositions, showing that, as a general trend, there is a blue-shift of the plasmon band during the reaction, but the plasmon band position levels off after some minutes. As a reference, the spectral evolution during the synthesis of pure Au nanoparticles is also shown in Fig. 2(d). The initial, intense band centred at *ca.* 313 nm is due to unreacted $AuCl_4^-$ ions. Comparison between all these spectral changes provides important information on the process of formation (see below).

Additional information on the process of particle formation is provided by TEM. Aliquots were taken from the sample during the formation of the alloy particles, quickly cooled down to stop the reaction, and a drop placed on a carbon coated TEM grid and blotted dry. A sequence of representative images for various stages of the process is shown in Fig. 3 for the same compositions as those in Fig. 2.

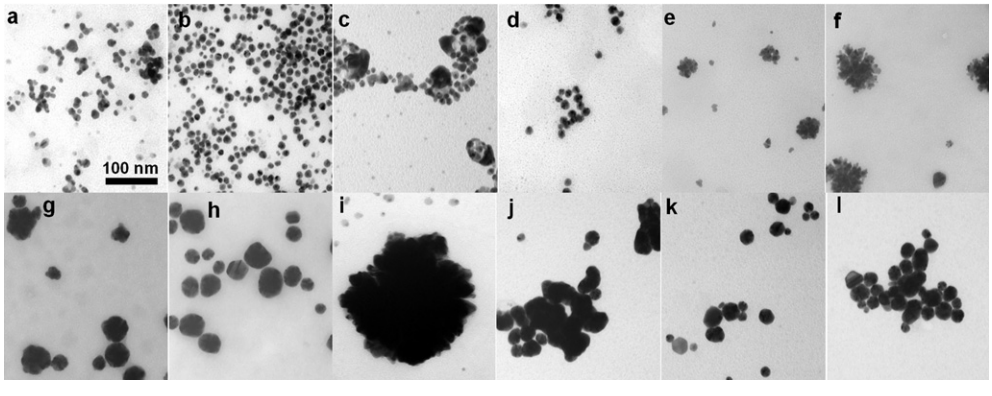

Fig. 3 TEM micrographs showing the evolution of the nanoparticles during the formation of an AuAg alloy with 25% Au (a–d), 50% Au (e–h), and 75% Au (i–l). Boiling times are 50 (a), 210 (b), 320 (c) 770 (d), 60 (e), 360 (f), 720 (g), 1170 (h), 15 (i), 460 (j), 610 (k), and 760 (l) seconds. The scale is the same for all images.

There are several aspects that differ between the formation of pure gold and the formation of gold–silver alloys, which are likely to arise from a different reduction rate, for the two metals. For the case with a larger amount of silver (75%), TEM indicates that nucleation is fast, leading to rapid formation of particles with similar particle size to that of the final alloy particles. However, EDS analysis at various stages shows that the atomic concentration of Au within the particles decreases during the process, which indicates that gold nuclei are initially formed, and silver is gradually reduced on the nuclei. HRTEM of the final particles does not reveal any distinct areas within the particles, thus suggesting a pure alloy morphology. The decrease in Au content within the nanoparticles agrees with the observed spectral changes, since there is a gradual blue shift from *ca.* 525 nm (corresponding to pure gold) until reaching a final value of 425 nm, which is much closer to that expected for pure Ag nanoparticles (400 nm).

Similar spectral changes were also observed for the other chosen compositions, but in a lower extent, due to the higher Au content in the final particles. TEM measurements show for both systems (50% and 75% Au) the initial coexistence of small particles together with larger blobs that seem to be aggregates formed by similar units. We have determined by EDS that the small nanoparticles are mainly made of silver, while the aggregates contain mostly gold. At later times (earlier for larger Au content) the small units seem to have fused together, and the aggregates appear more compact, eventually giving rise to separate nanoparticles, with a certain degree of polydispersity. The observation of large aggregates during citrate reduction is not new, since it was reported almost ten years ago by Chow and Zukoski[40] in a detailed study of the mechanism of gold sol formation by citrate reduction. These authors suggested the formation of a complex between the Au salt and the citrate ions, which was then slowly consumed to produce the final particles. In the context of the present paper, a similar mechanism can be suggested, where combination of Au and Ag atoms would rearrange to yield the final alloy nanoparticles. Such a mechanism would imply an equilibrium between particles and metal atoms/ions in solution, so that this lattice rearrangement can take place. Although the reaction temperature is only of the order of 100 °C, this may be sufficient to drive this process at the particle sizes considered. A similar mechanism was recently proposed by Klabunde and co-workers for the digestive ripening of metal nanoparticles.[41]

3.2. Interaction with ammonia

In this subsection, we describe the chemical modification of the AuAg alloy nanoparticles when ammonia is added to the colloid. As indicated in the introduction, while Au is not (chemically) affected by ammonia in solution, Ag nanoparticles readily dissolve according to eqn. (1). We are thus interested to find out whether complete dealloying takes place leading to pure Au nanoparticles.

The results are presented as time resolved spectroscopic studies and HRTEM images. Since the concentration of NH_4OH in solution affects the reaction rate, we have chosen a concentration (0.38 M) in a large excess with respect to the metal concentration (0.5 mM), but which still allows the colloid to be stable during the reaction.

The spectral evolution during the reaction is shown in Fig. 4(a)–(c) for three different alloy compositions. The general trend is a gradual damping and red-shift of the plasmon band, which is related to a selective oxidation of Ag atoms, as explained in the introduction. Not only the silver plasmon band is centred at 400 nm, while that for gold is at 520 nm, but also the extinction coefficient is of the order of 20 000 M^{-1} cm^{-1} for silver, but only 4000 M^{-1} cm^{-1} for gold.[13,42] An interesting observation is that even after six days, the silver component is not completely oxidised, *i.e.*, the plasmon band does not shift far enough to reach the position expected for pure Au nanoparticles. It can actually be observed (Fig. 4(d)) that the extent of the plasmon resonance shift increases with the silver content in the alloys: while for 25% Ag the shift is almost negligible (of the order of 1 nm, which is the resolution of the spectrophotometer) and is completed within a few minutes, a 7 nm shift is observed for 50% Ag within a few hours, and about 15 nm shift for 25% Ag, while there is still a slow shift after several days. The intensity drop of the plasmon band is also related to the silver content. We should note here that the change in composition inherent to the oxidation of silver atoms is not necessarily the only effect on the shape and position of the plasmon band. Since the reaction leads to the formation of positive $Ag(NH_3)_2^+$ ions, these can adsorb on the

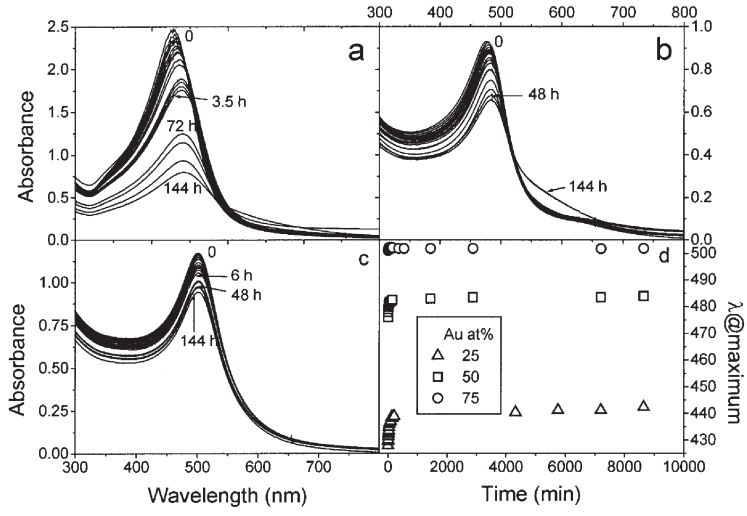

Fig. 4 (a)–(c) Spectral changes during the reaction of ammonia (0.38 M) with AuAg alloy colloids of various Au contents: 25% (a), 50% (b), and 75% (c). (d) Evolution of the maximum position during the reactions of cases (a)–(c).

particle surface, promoting a decrease in surface charge, which in turn leads to a red-shift and intensity drop of the plasmon band.[43,44]

Although the reason why no complete etching takes place is not perfectly clear, we propose the following model. In a perfect alloy structure, such as that expected for Au and Ag, which both crystallise in an fcc lattice with very close lattice constants (4.078 Å for Au, 4.086 Å for Ag), each Ag atom should be mostly surrounded by Au neighbours. This implies that, upon oxidation of a single Ag atom, the crystal lattice may rearrange, in a similar fashion to what happens for bulk alloys. However, whilst in bulk alloys surface energy minimization ultimately leads to a micro-porous structure,[38] in the case of nanoparticles, energy minimization tends to maintain a spherical geometry, and an outer Au shell may develop, which would protect the inner alloy sphere against further oxidation. Assuming that this model is correct, the protecting Au shell would be easier to form when the Ag concentration is lower, and thus particles with a higher silver content would be degraded in a larger extent, while for particles with a high gold content, the oxidation would be negligible.

The presence of Ag in the composition of the particles after long periods of time in contact with ammonia was confirmed by EDS. These results show that the silver concentration only slightly decreases, with a trend similar to what is observed in the spectroscopy studies. However, when the Ag concentration is very high ($>80\%$), a different situation is observed. For these particles, we occasionally see in HRTEM (see Fig. 5(a)) that a well-differentiated outer shell is surrounding a

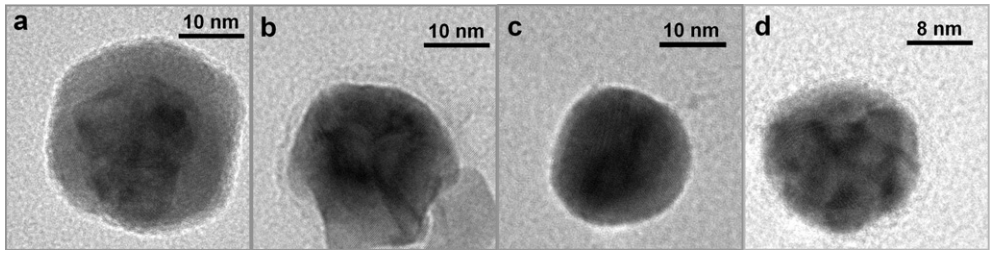

Fig. 5 High resolution transmission electron micrographs of AuAg alloy nanoparticles before (a,c) and after (b,d) reaction with ammonia in solution. The initial compositions were 15% Au (a,b) and 50% Au (c,d).

darker core, indicating that the particles are not pure alloys, but rather an alloy core coated by a silver shell. In those cases, ammonia oxidation leads to irregular shapes (Fig. 5(b)), which resemble the shape of the inner cores of the starting core-shell particles. For higher gold contents (see Fig. 5(c),(d) for 50% Au) the shape and average particle size remain basically unchanged after the etching process.

In summary, the selective etching of bimetallic AuAg nanoparticles does not lead to complete silver dissolution, which suggests that lattice rearrangement leads to the formation of a thin, protecting gold shell that prevents further oxidation. This protection is less effective as the silver content increases within the particles.

3.3. Silica coating

Silica coating has been long used to enhance the stability of a large variety of colloids. Apart from enhancing colloid stability, silica is chemically inert, optically transparent, and provides a suitable tool to tailor interparticle distance within nanoparticle assemblies, through control on shell thickness. A number of optical studies have been recently performed on silica coated gold nanoparticles ($Au@SiO_2$) and their assemblies.[37] Since for certain applications it is interesting to use metal nanoparticles with plasmon resonances at lower wavelengths and with higher extinction coefficients, it is desirable to be able to deposit silica shells of any desired thickness on AuAg alloys with a variable concentration. However, we have demonstrated in a previous study[35] that silica coating of pure Ag nanoparticles with thick silica shells is strongly limited due to complete etching of the silver cores through aerial oxidation catalysed by ammonia during growth by means of the Stöber process.[34] In the previous section we have shown that when the silver content is not extremely high, the reaction with ammonia only leads to partial etching, and the plasmon band position is not strongly influenced. This means that silica coating can be performed on the alloy nanoparticles, basically maintaining their optical properties. As an example, we have monitored the silica coating of an alloy colloid with 50% Au and 50% Ag. Shown in Fig. 6 are transmission electron micrographs of the nanoparticles during various stages of the silica coating process. The coating is performed through the same procedure designed for pure Au nanoparticles,[36] and comprises initially the priming of the metal core surface with the silane coupling agent 3-aminopropyltrimethoxysilane (APS), followed by slow deposition of a thin, homogeneous silica shell by addition of sodium silicate solution at $pH \approx 8$ (see Fig. 6(a)). Once this thin shell has been deposited, the particles are transferred into ethanol, so that the excess silicate condenses, mainly on the coated metal cores, and partly forming new silica nuclei (Fig. 6(b)), which can be separated by centrifugation. Redispersion in ethanol and addition of ammonia and TEOS leads to the growth of the silica shells, although occasionally multiple cores have been observed (Fig. 6(c)).

The spectral evolution during silica coating is shown in Fig. 7. The deposition of the initial silica shell promotes a red-shift of the plasmon band due to an increase in the local refractive index around the metal cores.[23] A further red shift is observed upon transfer into ethanol for the same reason (refractive index of ethanol is larger than for water, and the shell thickness is increased), which agrees with predictions by Mie theory, as was previously shown for $Au@SiO_2$.[36] When the silica shells are much thicker, light scattering is the most predominant optical effect, and the plasmon band is only observed as a bump within a typical Rayleigh scattering curve. However, a further red shift was observed in this case, opposite to what was previously found for Au cores, which is very likely due to partial etching by the ammonia used to catalyse TES hydrolysis and condensation. Ammonia concentration in this case is only slightly lower to that used in the selective etching experiments reported in the previous section.

3.4. Sol–gel processing

As a consequence of the silica coating work previously mentioned, we have recently developed two alternative procedures to prepare silica gels and monoliths in which silica coated gold nanoparticles are uniformly distributed.[45] Both methods rely on the presence of silica on the surface on the nanoparticles, thus imparting to the metal nanoparticles with basically identical surface composition and properties as those of the silica particles formed and assembled during the sol–gel process.[45,46] One of the methods consists of mixing a solution of sodium silicate with an aqueous

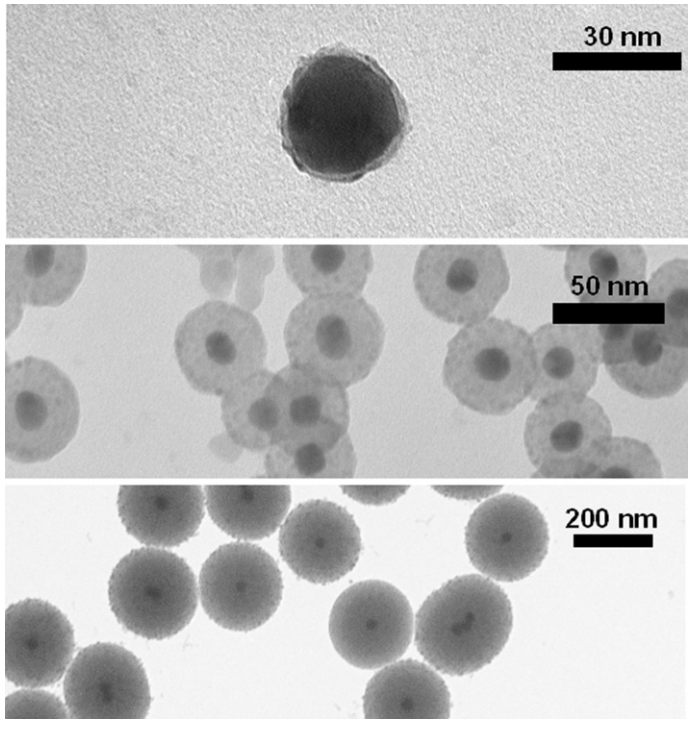

Fig. 6 Transmission electron micrographs of AuAg alloy nanoparticles (Au content = 50 atom%) coated with silica shells of various thicknesses.

colloid of the coated nanoparticles, followed by pH adjustment to *ca.* 7 with HCl, while the second is performed in water/methanol mixtures, through the hydrolysis and condensation of tetramethoxysilane (TMOS) catalysed by excess citrate. We demonstrated[47] that the optical properties of the constituting nanoparticles are retained in both types of gels, though those obtained through TMOS hydrolysis are more transparent (less turbid), which is more convenient for most

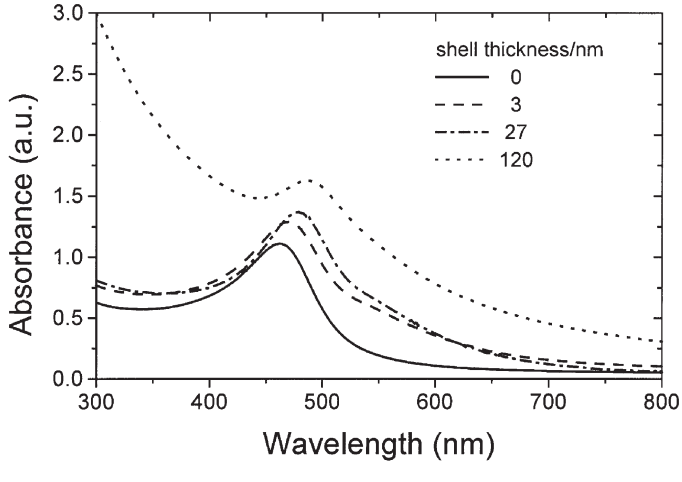

Fig. 7 UV–visible spectra of AuAg@SiO_2 nanoparticles for various shell thicknesses.

applications. Upon drying, solid and transparent coloured glasses are obtained, which show interesting nonlinear optical properties.[48]

Any of these processes can also be performed using AuAg alloy nanoparticles, which means that solid glass with optical properties determined by the composition of the alloy nanoparticles can be easily prepared. This can be of relevance for a number of applications, such as optical filters, decorative glasses, or materials with non-linear optical properties.

Examples are provided in Fig. 8, where the spectral evolution during sol–gel processing is shown for two alloy colloids with different composition. In the figure it can be clearly observed that the maximum position remains constant (438.5 nm for 25% Au; 464 nm for 50% Au), and the only change is a slight increase in light scattering (reflected in a Rayleigh-like contribution), due to the formation of micropores within the gel structure. Upon drying, the hydrogels compress and lead to formation of xerogels, which are transparent and display uniform colours. The homogeneous distribution of the alloy nanoparticles within the xerogels has been confirmed by TEM, as exemplified in the insets within Fig. 8 for 25 and 50% Au, and at different magnifications. The precise position of the plasmon band in the dry gels is slightly red-shifted as compared to the wet hydrogels due to a further increase in the average refractive index due to pore compression.

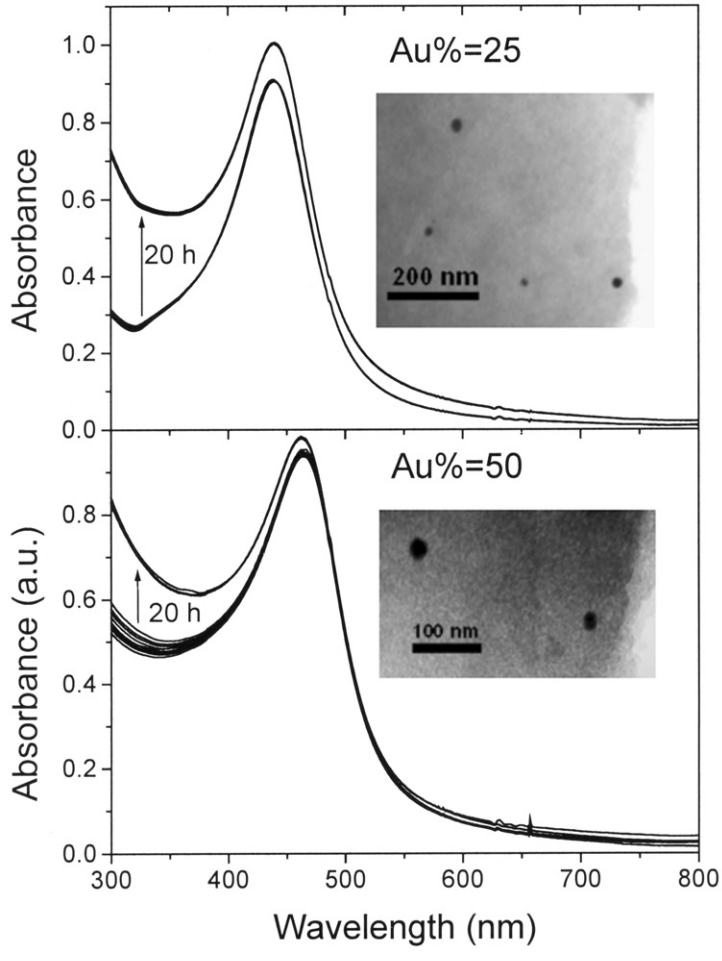

Fig. 8 Time evolution of UV-visible spectra during sol–gel processing of AuAg@SiO_2 nanoparticles for two different particle compositions. The insets show representative TEM images of the doped gels.

Conclusions

The time resolved study of the simultaneous reduction of gold and silver salts with citrate ions indicates that the mechanism involves separate nucleation of both metals, and further rearrangement that leads to uniform alloy particles. TEM results suggest that gold is reduced first, and the relative amount of silver within the alloy nanoparticles increases with time until reaching the final values. The reaction of alloy nanoparticles with ammonia showed that the silver atoms close to the nanoparticle surface easily get oxidized, while the reaction is never complete, since reorganization of the gold atoms leads to formation of a gold shell that prevents ammonia molecules from entering the inner part of the particles. This protection allows the deposition of both thin and thick silica shells on the alloy particles, as well as their uniform incorporation within silica gels which retain the spectral features of the starting alloy dilute colloid.

Acknowledgements

The authors would like to thank Dr Isabel Pastoriza-Santos for fruitful discussions, and Uli Bloeck for performing HRTEM and EDS measurements. This work has been supported by the Spanish Xunta de Galicia (Project No. PGIDT01PXI30106PR), and Ministerio de Ciencia y Tecnología (Project No. BQU2001-3799). A.S.-I. acknowledges receipt of a scholarship from Universidade de Vigo.

References

1 M. Faraday, *Philos. Trans. R. Soc. London*, 145, **147**, 1857.
2 J. Turkevich, P. C. Stevenson and J. Hillier, *Discuss. Faraday. Soc.*, 1951, **11**, 55.
3 L. D. Rampino and F. F. Nord, *J. Am. Chem. Soc.*, 1941, **63**, 2745.
4 R. H. Doremus, *J. Chem. Phys.*, 1965, **42**, 414.
5 G. Schmid and A. Lehnert, *Angew. Chem., Int. Ed. Engl.*, 1989, **28**, 780.
6 S. M. Heard, F. Grieser, C. G. Barraclough and J. V. Sanders, *J. Colloid Interface Sci.*, 1983, **93**, 545.
7 C. Petit, P. Lixon and M. P. Pileni, *J. Phys. Chem.*, 1993, **97**, 12 974.
8 A. Henglein, *J. Phys. Chem.*, 1993, **97**, 5457.
9 P. A. Buining, B. M. Humbel, A. P. Philipse and A. J. Verkleij, *Langmuir*, 1997, **13**, 3921.
10 M. Brust, M. Walker, D. Bethell, D. J. Schiffrin and R. Whyman, *J. Chem. Soc., Chem. Commun.*, 1994, 801.
11 I. Pastoriza-Santos and L. M. Liz-Marzán, *Langmuir*, 1999, **15**, 948.
12 A. Henglein, A. Holzwarth and P. Mulvaney, *J. Phys. Chem.*, 1992, **96**, 8700.
13 P. Mulvaney, M. Giersig and A. Henglein, *J. Phys. Chem.*, 1993, **97**, 7061.
14 A. Henglein and M. Giersig, *J. Phys. Chem.*, 1994, **98**, 6931.
15 A. F. Lee, C. J. Baddeley, C. Hardacre, R. M. Ormerod, R. M. Lambert, G. Schmid and H. West, *J. Phys. Chem.*, 1995, **99**, 6096.
16 L. M. Liz-Marzán and A. P. Philipse, *J. Phys. Chem.*, 1995, **99**, 15 120.
17 N. Toshima and T. Yonezawa, *New J. Chem.*, 1998, **22**, 1179.
18 A. Henglein and M. Giersig, *J. Phys. Chem. B*, 2000, **104**, 5056.
19 U. Kreibig, M. Vollmer, *Optical Properties of Metal Clusters*, Springer, Berlin, 1995.
20 G. Mie, *Ann. Phys.*, 1908, **25**, 337.
21 C. F. Bohren, D. Huffman, *Absorption and Scattering of Light by Small Particles*, Wiley, New York, 1983.
22 M. Kerker, *The Scattering of Light and Other Electromagnetic Radiation*, Academic Press, New York, 1969.
23 P. Mulvaney, *Langmuir*, 1996, **12**, 788.
24 J. A. Creighton, C. G. Blatchford and M. G. Albrecht, *J. Chem. Soc., Faraday Trans. 2*, 1979, **75**, 790.
25 R. H. Morriss and L. F. Collins, *J. Chem. Phys.*, 1964, **41**, 3357.
26 A. Henglein, *J. Phys. Chem. B*, 2000, **104**, 2201.
27 F. Henglein, A. Henglein and P. Mulvaney, *Ber. Bunsenges. Phys. Chem.*, 1994, **98**, 180.
28 L. Rivas, S. Sánchez-Cortes, J. V. García-Ramos and G. Morcillo, *Langmuir*, 2000, **16**, 9722.
29 Y. W. Cao, R. Jin and C. A. Mirkin, *J. Am. Chem. Soc.*, 2001, **123**, 7961.
30 J. Marignier, J. Belloni, M. Delcourt and J. Chevalier, *Nature*, 1985, **317**, 344.
31 S. Link, Z. L. Wang and M. A. El-Sayed, *J. Phys. Chem. B*, 1999, **103**, 3529.
32 M. P. Mallin and C. J. Murphy, *Nano Lett.*, 2002, **2**, 1235.
33 M. Giersig, T. Ung, L. M. Liz-Marzán and P. Mulvaney, *Adv. Mater.*, 1997, **9**, 570.
34 W. Stöber, A. Fink and E. Bohn, *J. Colloid Interface Sci.*, 1968, **26**, 62.
35 T. Ung, L. M. Liz-Marzán and P. Mulvaney, *Langmuir*, 1998, **14**, 3740.

36 L. M. Liz-Marzán, M. Giersig and P. Mulvaney, *Langmuir*, 1996, **12**, 4329.
37 P. Mulvaney and L. M. Liz-Marzán, *Top. Curr. Chem.*, 2003, **126**, 125.
38 J. Erlebacher, M. J. Aziz, A. Karma, N. Dimitrov and K. Sieradzki, *Nature*, 2001, **410**, 450.
39 K. Ripken, *Z. Phys.*, 1972, **250**, 228.
40 M. K. Chow and C. F. Zukoski, *J. Colloid Interface Sci.*, 1994, **165**, 97.
41 B. L. V. Prasad, S. I. Stoeva, C. M. Sorensen and K. J. Klabunde, *Chem. Mater.*, 2003, **15**, 935.
42 M. Carey Lea, *Am. J. Sci.*, 476, **37**, 1889.
43 T. Ung, D. Dunstan, M. Giersig and P. Mulvaney, *Langmuir*, 1997, **13**, 1773.
44 T. Ung, L. M. Liz-Marzán and P. Mulvaney, *J. Phys. Chem.*, 1999, **103**, 6770.
45 R. K. Iler, *The Chemistry of Silica*, John Wiley & Sons, New York, 1979.
46 C. J. Brinker, and G. W. Scherer, *Sol–Gel Science*, Academic Press, San Diego, 1990.
47 Y. Kobayashi, M. A. Correa-Duarte and L. M. Liz-Marzán, *Langmuir*, 2001, **17**, 6375.
48 S. Tamil-Selvan, T. Hayakawa, M. Nogami, Y. Kobayashi, L. M. Liz-Marzán, Y. Hamanaka and A. Nakamura, *J. Phys. Chem. B*, 2002, **106**, 10 157.